Inorganic Chemistry

Article

pubs.acs.org/IC

Construction of the Tetrahedral Trifluorophosphine Platinum Cluster $Pt_4(PF_3)_8$ from Smaller Building Blocks

Peigang Hu,[†] Qiong Luo,*[,†] Qian-shu Li,[†] Yaoming Xie,[‡] R. Bruce King,*[,†,‡] and Henry F. Schaefer[‡]

[†]MOE Key Laboratory of Theoretical Environmental Chemistry, Center for Computational Quantum Chemistry, South China Normal University, Guangzhou 510631, P. R. China

[‡]Department of Chemistry and Center for Computational Chemistry, University of Georgia, Athens, Georgia 30602, United States

Supporting Information

ABSTRACT: The experimentally known but structurally uncharacterized $Pt_4(PF_3)_8$ is predicted to have an S_4 structure with a central distorted Pt_4 tetrahedron having four short Pt═Pt distances, two long Pt−Pt distances, and all terminal PF_3 groups. The structures of the lower nuclearity species $Pt(PF_3)_n$ (n = 4, 3, 2), $Pt_2(PF_3)_n$ (n = 7, 6, 5, 4), and $Pt_3(PF_3)_6$ were investigated by density functional theory to assess their possible roles as intermediates in the formation of $Pt_4(PF_3)_8$ by the pyrolysis of $Pt(PF_3)_4$. The expected tetrahedral, trigonal planar, and linear structures are found for $Pt(PF_3)_4$, $Pt(PF_3)_3$, and $Pt(PF_3)_2$, respectively. However, the dicoordinate $Pt(PF_3)_2$ structure is bent from the ideal 180° linear structure to approximately 160°. Most of the low-energy binuclear $Pt_2(PF_3)_n$ (n = 7, 6, 5) structures can be derived from the mononuclear $Pt(PF_3)_n$ (n = 4, 3, 2) structures by replacing one of the PF_3 groups by a $Pt(PF_3)_4$ or $Pt(PF_3)_3$ ligand. In some of these binuclear structures one of the PF_3 groups on the $Pt(PF_3)_n$ ligand becomes a bridging group. The low-energy binuclear structures also include symmetrical $[Pt(PF_3)_n]_2$ dimers (n = 2, 3) of the coordinately unsaturated $Pt(PF_3)_n$ (n = 3, 2). The four low-energy structures for the trinuclear $Pt_3(PF_3)_6$ include two structures with central equilateral Pt_3 triangles and two structures with isosceles Pt_3 triangles and various arrangements of terminal and bridging PF_3 groups. Among these four structures the lowest-energy $Pt_3(PF_3)_6$ structure has an unprecedented four-electron donor η^2-μ_3-PF_3 group bridging the central Pt_3 triangle through three Pt−P bonds and one Pt−F bond. Thermochemical studies on the aggregation of these Pt-PF_3 complexes suggest the tetramerization of $Pt(PF_3)_2$ to $Pt_4(PF_3)_8$ to be highly exothermic regardless of the mechanistic details.

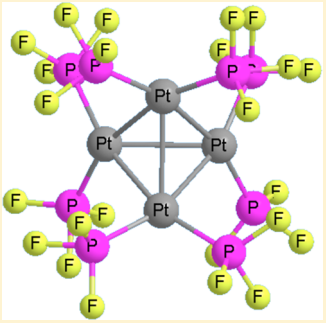

1. INTRODUCTION

Trifluorophosphine (PF_3) is a strong π-acceptor ligand that can stabilize low formal oxidation states in a manner similar to carbon monoxide.[1−10] In fact, the homoleptic zerovalent metal derivatives, such as $Cr(PF_3)_6$, $Fe(PF_3)_5$, and $Ni(PF_3)_4$, are even more thermally and oxidatively stable than the corresponding homoleptic metal−carbonyls.[11,12] This greater stability of zerovalent $M(PF_3)_n$ complexes relative to corresponding $M(CO)_n$ complexes has allowed the synthesis of some zerovalent metal trifluorophosphine complexes that do not have stable metal−carbonyl analogues.

Of particular interest is the platinum trifluorophosphine complex $Pt(PF_3)_4$, which is a stable volatile liquid in contrast to the unstable $Pt(CO)_4$. In fact, $Pt(PF_3)_4$ has been used for the chemical vapor deposition of platinum metal.[13−16] Furthermore, laboratory exploration of the pyrolysis of $Pt(PF_3)_4$ has resulted in the discovery of an intriguing stable tetranuclear zerovalent platinum trifluorophosphine $Pt_4(PF_3)_8$, which has no counterpart in the chemistry of platinum carbonyls or zerovalent nickel carbonyl or nickel trifluorophosphine derivatives.[17] Although $Pt_4(PF_3)_8$ is reported to be a yellow solid, efforts to obtain suitable single crystals for a definitive structural determination by X-ray crystallography so far have been unsuccessful.

The well-known 18-electron rule for the stability of low oxidation state d-block transition-metal complexes[18−22] does not apply as rigorously to the zerovalent chemistry of the late transition metals, particularly platinum. Thus, the observed stable zerovalent platinum complexes include not only 18-electron complexes of the type PtL_4 (L = two-electron donor ligand) but also 16-electron complexes of the type PtL_3 and even 14-electron complexes of the type PtL_2.[23] It is therefore conceivable that the formation of $Pt_4(PF_3)_8$ by the pyrolysis of $Pt(PF_3)_4$ first proceeds by successive trifluorophosphine loss to give $Pt(PF_3)_3$ and then $Pt(PF_3)_2$. Tetramerization of $Pt(PF_3)_2$ would then lead to $Pt_4(PF_3)_8$.

We used density functional theory (DFT) to explore the preferred structures of these zerovalent platinum trifluorophosphine complexes as well as the thermochemistry of plausible sequences of reactions leading to $Pt_4(PF_3)_8$. We find that an interesting distorted tetrahedral structure with S_4 point group symmetry for $Pt_4(PF_3)_8$ lies more than 24 kcal/mol in energy below any other $Pt_4(PF_3)_8$ structures and thus is the likely structure of the $Pt(PF_3)_4$ laboratory pyrolysis product. Furthermore, the thermochemistry for the tetramerization of $Pt(PF_3)_2$ to $Pt_4(PF_3)_8$ is found to be favorable despite the

Received: March 6, 2014
Published: May 6, 2014

dx.doi.org/10.1021/ic5005243 | Inorg. Chem. 2014, 53, 5300−5310

known existence of stable PtL_2 complexes with other types of ligands such as tertiary phosphines. Also we find bridging PF_3 groups to be a common feature in low-energy binuclear $Pt_2(PF_3)_n$ (n = 7, 6, 5, 4) structures as well as trinuclear $Pt_3(PF_3)_6$ structures. Bridging PF_3 groups are generally found to be much rarer in the chemistry of metal trifluorophosphine complexes than bridging CO groups in the chemistry of metal–carbonyl complexes.

2. THEORETICAL METHODS

Electron-correlation effects were included by employing DFT methods, which have evolved as a practical and effective computational tool, especially for organometallic compounds.[24−30] Two DFT methods, namely BP86 and MPW1PW91, were used in this study. The BP86 method is a pure DFT method that combines Becke's 1988 exchange functional with Perdew's 1986 correlation functional.[31,32] The MPW1PW91 method,[33] based on the generalized gradient approximation (GGA), is a newer density functional and may be more suitable for the second- and third-row transition-metal systems.[34]

For the third-row transition metals, the large numbers of electrons increase exponentially the computational efforts. To reduce the cost, the Stuttgart/Dresden effective core potential (ECP) basis sets are employed.[35] The ECP also includes relativistic effects, which are important for the heavy transition-metal atoms. With this ECP basis set, the 60 electrons in the lowest spin–orbitals (1s to 4f) for the platinum atoms are replaced by an effective core potential, and the valence basis set is contracted from (8s7p6d) primitive sets to (6s5p3d). For the fluorine and phosphorus atoms the all-electron double-ζ plus polarization (DZP) basis sets are employed. These add one set of pure spherical harmonic d functions with orbital exponents $\alpha_d(F)$ = 1.0 and $\alpha_d(P)$ = 0.6 to the Huzinaga–Dunning standard contracted DZ sets[36−38] and are designated (9s5p1d/4s2p1d) for fluorine and (11s7p1d/6s4p1d) for phosphorus.

The geometries of all structures were fully optimized using the DFT methods BP86 and MPW1PW91. The vibrational frequencies and the corresponding infrared intensities were determined analytically. All of the computations were carried out with the Gaussian 09 program,[39] in which the (75, 302) grid is the default for evaluating integrals numerically. The finer (99, 590) grid is used for evaluating the imaginary vibrational frequencies.

In the search for minima using all currently implemented DFT methods, low-magnitude imaginary vibrational frequencies are suspect because of significant limitations in the numerical integration procedures used in the DFT computations.[40] Thus, all imaginary vibrational frequencies with magnitudes less than 50i cm^{-1} are considered questionable, and are given less weight in the analysis.[41,42] Therefore, we do not always follow such low imaginary vibrational frequencies. In the present research, only singlet structures are discussed, since the triplet structures were found to have much higher energies than the corresponding singlets. All of the structures reported here have substantial highest occupied molecular orbital–lowest unoccupied molecular orbital (HOMO–LUMO) gaps of at least 2 eV (BP86) or 4 eV (MPW1PW91), as indicated in the Tables.

3. RESULTS

3.1. Structure of the Tetranuclear Derivative $Pt_4(PF_3)_8$. The tetranuclear derivative $Pt_4(PF_3)_8$ was first prepared in 1997 by Clark et al., and its composition has been confirmed by Fourier transform ion cyclotron resonance mass spectrometry.[17] However, its geometry is still unknown since suitable single crystals were not obtained for X-ray crystallography. To predict the structure of $Pt_4(PF_3)_8$, starting structures with tetrahedral, butterfly, and square arrangements of the central Pt_4 unit having six, five, and four Pt–Pt bonds, respectively, were optimized using DFT. However, the energies of the structures with central butterfly and square Pt_4 units were found to lie more than 20 kcal/mol above the tetrahedral structure. Thus, only the tetrahedral structure is reported here (Figure 1). This structure **48S-1** has the rather rare S_4 symmetry point group with all terminal PF_3 groups. Four of the Pt–P distances are 2.235 Å (BP86) or 2.208 Å (MPW1PW91), whereas the other four Pt–P distances are 2.249 Å (BP86) or 2.229 Å (MPW1PW91). The predicted four short Pt=Pt bond distances are 2.655 Å (BP86) or 2.634 Å (MPW1PW91), and the two long Pt–Pt bond distances are 2.903 Å (BP86) or 2.904 Å (MPW1PW91). These Pt–Pt distances suggest four formal double bonds and two formal single bonds in the Pt_4 tetrahedron. Optimization of the $Pt_4(PF_3)_8$ structure with the nonrelativistic all-electron basis set mDZP of Paschoal et al.[43] gave essentially the same structure but with Pt–Pt distances ~0.03 Å longer.

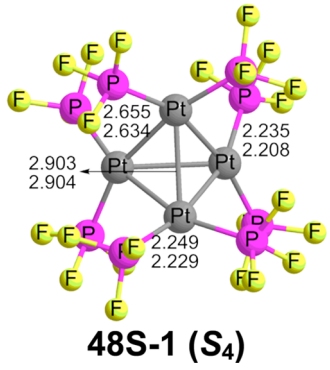

Figure 1. The optimized $Pt_4(PF_3)_8$ structure. Bond distances in Å are reported from two theoretical methods, namely, BP86 (upper) and MPW1PW91 (lower).

3.2. Structures of the Mononuclear Derivatives. *3.2.1. $Pt(PF_3)_4$.* The only structure found for the coordinately saturated 18-electron complex $Pt(PF_3)_4$ is the expected tetrahedral structure **14S-1** (Figure 2), which is a genuine minimum. The predicted Pt–P bond length of 2.276 Å (BP86) or 2.255 Å (MPW1PW91) agrees well the experimental Pt–P distance of 2.229(5) Å in $Pt(PF_3)_4$, as determined via gas-phase electron diffraction by Ritz and Bartell.[44]

3.2.2. $Pt(PF_3)_3$. The only structure found for the coordinately unsaturated 16-electron complex $Pt(PF_3)_3$ is the trigonal planar C_{3h} structure **13S-1** with equivalent Pt–P distances of 2.246 Å (BP86) or 2.232 Å (MPW1PW91) (Figure 2). Structure **13S-1** has three small imaginary vibrational frequencies at 18i, 16i, and 16i cm^{-1} (BP86) or 19i, 16i, and 16i cm^{-1} (MPW1PW91). However, these imaginary frequencies appear to arise from numerical error in the integration process, since they were removed using the finer (99, 590) integration grid.[40]

3.2.3. $Pt(PF_3)_2$. Only one singlet structure **12S-1** is found for the highly coordinately unsaturated 14-electron complex $Pt(PF_3)_2$ (Figure 2). This C_2 structure **12S-1** is a genuine minimum with no imaginary vibrational frequencies. The Pt–P distances in **12S-1** are 2.205 Å (BP86) or 2.200 Å (MPW1PW91), and the P–Pt–P angle is 155.8° (BP86) or 161.2° (MPW1PW91).

3.3. Structures of the Binuclear Derivatives. *3.3.1. The Saturated Structure $Pt_2(PF_3)_7$.* Two low-lying singlet $Pt_2(PF_3)_7$ structures were found (Figure 3 and Table 1). The global minimum **27S-1** is a C_{3v} structure composed of $Pt(PF_3)_3$ and $Pt(PF_3)_4$ units linked by a Pt–Pt bond. The Pt–Pt distance of 3.025 Å (BP86) or 2.987 Å (MPW1PW91) corresponds to a weak Pt–Pt single bond to give the platinum atoms in both the

dx.doi.org/10.1021/ic5005243 | Inorg. Chem. 2014, 53, 5300−5310

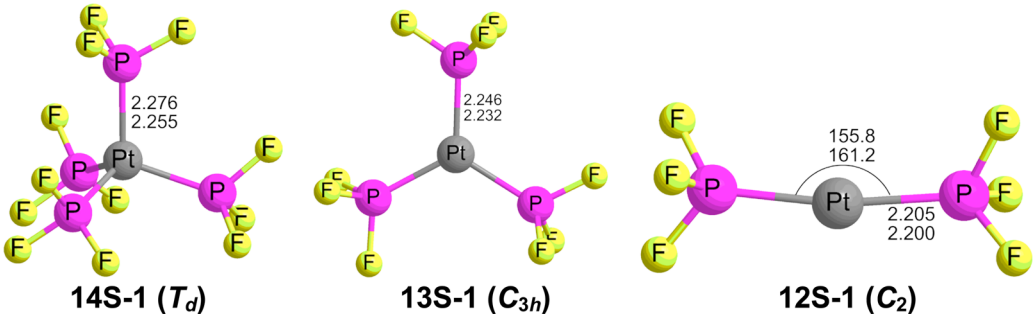

Figure 2. The optimized structures of $Pt(PF_3)_n$ (n = 4, 3, and 2). Bond distances in Å are reported from two theoretical methods, namely, BP86 (upper) and MPW1PW91 (lower).

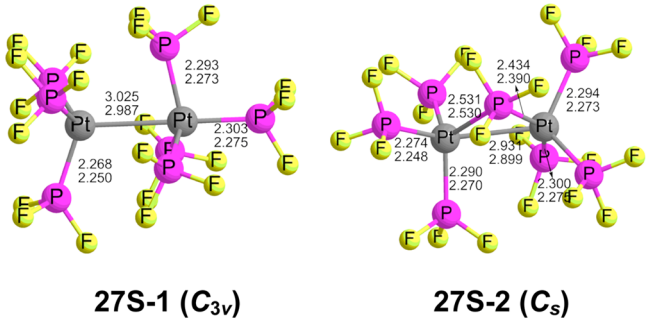

Figure 3. The two optimized $Pt_2(PF_3)_7$ structures.

Table 1. Selected Data for the Optimized $Pt_2(PF_3)_7$ Structures

	parameter	**27S-1** (C_{3v})	**27S-2** (C_s)
BP86	E^a	−4726.772 90	−4726.766 69
	ΔE^b	0.0	3.9
	gap^c	3.25	3.32
	Pt−Pt^d	3.051	2.931
	$N_{imag}{}^e$	1 (15i)	2 (29i, 12i)
MPW1PW91	E	−4725.962 13	−4725.952 38
	ΔE	0.0	6.1
	gap	5.24	5.23
	Pt−Pt	2.987	2.899
	N_{imag}	none	3 (30i, 11i, 8i)

^{a}Total energies (E in Hartree). ^{b}Relative energies (ΔE in kcal/mol). ^{c}HOMO−LUMO gaps (in eV). ^{d}Pt−Pt distances (in Å). ^{e}Numbers of imaginary frequencies.

$Pt(PF_3)_3$ and $Pt(PF_3)_4$ units the favored 18-electron configurations. Structure **27S-1** has one tiny imaginary vibrational frequency at 15i cm^{-1} by the BP86 method. However, it has all real harmonic vibrational frequencies by the MPW1PW91 method.

The second $Pt_2(PF_3)_7$ structure **27S-2**, lying 3.9 kcal/mol (BP86) or 6.1 kcal/mol (MPW1PW91) in energy above **27S-1**, has two very small imaginary vibrational frequencies at 29i and 12i cm^{-1} (BP86) or three very small imaginary vibrational frequencies at 30i, 11i, and 8i cm^{-1} (MPW1PW91). Structure **27S-2** is a C_s structure composed of two $Pt(PF_3)_3$ units linked by a bridging PF_3 group and a direct Pt−Pt bond (Figure 3 and Table 1). The bridging PF_3 group in **27S-2** is unsymmetrical, with a short Pt−P distance of 2.434 Å (BP86) or 2.390 Å (MPW1PW91) and a long Pt−P distance of 2.531 Å (BP86) or 2.530 Å (MPW1PW91). The Pt−Pt distance of 2.931 Å (BP86) or 2.899 Å (MPW1PW91) in **27S-2** suggests the formal single bond required to give each platinum atom the favored 18-electron configuration. The Pt−Pt bond in **27S-2** is ∼0.1 Å shorter than that in **27S-1**, owing to the effect of the bridging PF_3 group in the former.

3.3.2. $Pt_2(PF_3)_6$. Three low-lying singlet structures were found for $Pt_2(PF_3)_6$ (Figure 4 and Table 2). Their energies are closely spaced within 5 kcal/mol in energy, suggesting a potentially fluxional system. The lowest-energy structure is **26S-1** with the unusual S_6 point group consisting of two $Pt(PF_3)_3$ units linked by a weak Pt−Pt bond of length 3.090 Å (BP86) or 3.141 Å (MPW1PW91).

The second $Pt_2(PF_3)_6$ structure **26S-2**, lying only 2.4 kcal/mol (BP86) or 0.9 kcal/mol (MPW1PW91) in energy above **26S-1**, is asymmetric, consisting of a $Pt(PF_3)_4$ unit and a $Pt(PF_3)_2$ unit linked by a direct Pt−Pt bond (Figure 4 and

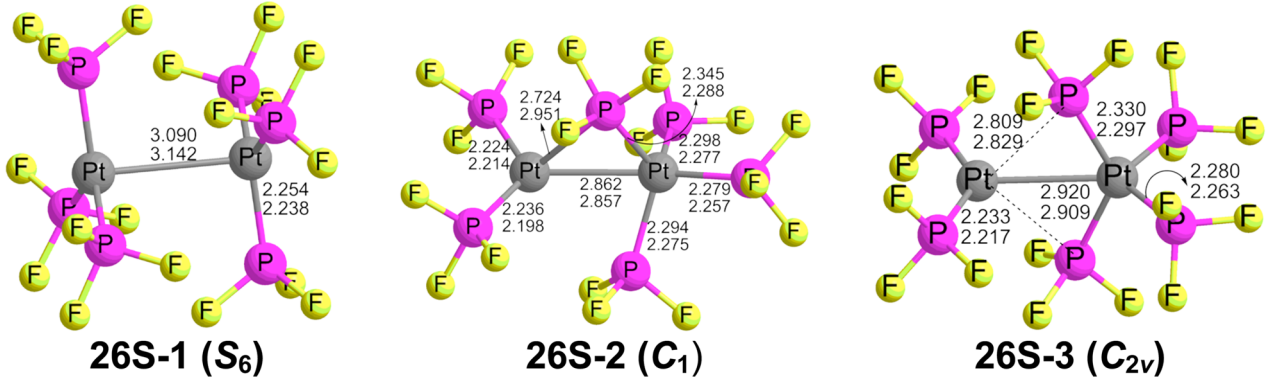

Figure 4. The three optimized $Pt_2(PF_3)_6$ structures.

dx.doi.org/10.1021/ic5005243 | *Inorg. Chem.* 2014, 53, 5300−5310

Table 2. Selected Data for the Optimized $Pt_2(PF_3)_6$ Structures

		26S-1 (S_6)	26S-2 (C_1)	26S-3 (C_{2v})[a]
BP86	E[b]	−4085.679 34	−4085.675 50	−4085.674 37
	ΔE[c]	0.0	2.4	3.1
	gap[d]	2.39	2.83	2.79
	Pt−Pt[e]	3.090	2.862	2.920
	N_{imag}[f]	none	none	2(8*i*,6*i*)
MPW1PW91	E	−4084.951 37	−4084.949 87	−4084.946 19
	ΔE	0.0	0.9	3.2
	gap	4.18	4.90	4.68
	Pt−Pt	3.141	2.857	2.908
	N_{imag}	none	none	3(10*i*,10*i*,10*i*)

[a]Using a finer integration grid (99, 590), only one tiny imaginary frequency of 10*i* cm^{-1} (BP86) or 15*i* cm^{-1} (MPW1PW91) was obtained. [b]Total energies (E in Hartree). [c]Relative energies (ΔE in kcal/mol). [d]HOMO−LUMO gaps (in eV). [e]Pt−Pt distances (in Å). [f]Numbers of imaginary frequencies.

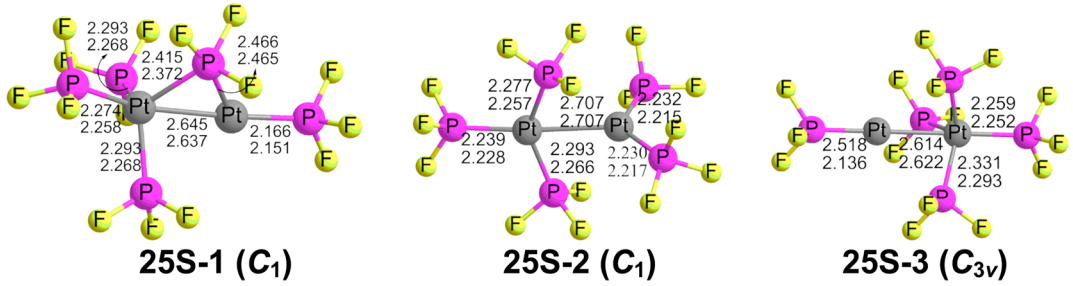

Figure 5. The three optimized $Pt_2(PF_3)_5$ structures.

Table 3. Selected Data for the Optimized $Pt_2(PF_3)_5$ Structures

		25S-1 (C_s)[a]	25S-2 (C_1)	25S-3 (C_{3v})
BP86	E[b]	−3444.582 41	−3444.581 07	−3444.579 96
	ΔE[c]	0.0	0.8	1.5
	gap[d]	3.37	2.83	3.88
	Pt−Pt[e]	2.645	2.707	2.614
	N_{img}[f]	2 (22*i*,14*i*)	none	4 (30*i*,30*i*,25*i*,10*i*)
MPW1PW91	E	−3443.943 69	−3443.941 59	−3443.941 51
	ΔE	0.0	1.3	1.4
	gap	5.34	4.54	5.80
	Pt−Pt	2.637	2.707	2.622
	N_{img}	1 (16*i*)	none	4 (26*i*,21*i*,21*i*,5*i*)

[a]The imaginary frequency of this structure can be removed by using the finer (99, 590) integration grid. [b]Total energies (E in Hartree). [c]Relative energies (ΔE in kcal/mol). [d]HOMO−LUMO gaps (in eV). [e]Pt−Pt distances (in Å). [f]Numbers of imaginary vibrational frequencies.

Table 2). Structure **26S-2** can be regarded as a substitution product of $Pt(PF_3)_3$ in which one of the PF_3 ligands has been replaced by a trihapto $Pt(PF_3)_4$ ligand bonding to the other platinum atom through a Pt→Pt dative bond, which is predicted to be 2.862 Å (BP86) or 2.857 Å (MPW1PW91) in length. Thus, the Pt atom in the $Pt(PF_3)_4$ unit has the favorable 18-electron configuration, and the Pt atom in the $Pt(PF_3)_2$ unit has a 16-electron configuration, if the Pt→Pt dative bond is considered as a formal single bond in accord with its length.

The third $Pt_2(PF_3)_6$ structure **26S-3**, lying 3.1 kcal/mol (BP86) or 3.2 kcal/mol (MPW1PW91) in energy above **26S-1**, is geometrically similar to **26S-2** but with the constraint of C_{2v} symmetry (Figure 4 and Table 2). Thus, **26S-3**, like **26S-2**, has a $Pt(PF_3)_4$ unit and a $Pt(PF_3)_2$ unit linked by a dative Pt→Pt bond of length 2.920 Å (BP86) or 2.909 Å (MPW1PW91). In **26S-3** the Pt atom in the $Pt(PF_3)_4$ unit has the favored 18-electron configuration, whereas the other Pt atom has only a 16-electron configuration, similar to the Pt atom in **13S-1** (Figure 2). Structure **26S-3** has two (BP86) or three (MPW1PW91) very small imaginary vibrational frequencies. The finer integration grid (99, 590) reduces them to one tiny imaginary frequency of 10*i* cm^{-1} (BP86) or 15*i* cm^{-1} (MPW1PW91). Following the related normal mode results in the distortion of C_{2v} symmetry to C_1 symmetry, leading to **26S-2**.

3.3.3. $Pt_2(PF_3)_5$. Three low-lying $Pt_2(PF_3)_5$ structures were found having relative energies within 1.5 kcal/mol, suggesting a potentially fluxional system similar to that of $Pt_2(PF_3)_6$ (Figure 5 and Table 3). Structure **25S-1** has a $Pt(PF_3)_3$ unit and a $Pt(PF_3)$ unit, linked by a Pt−Pt bond and a bridging PF_3 group. It has tiny imaginary vibrational frequencies, either 22*i* and 14*i* cm^{-1} (BP86) or 6*i* cm^{-1} (MPW1PW91). However, these imaginary frequencies arise from numerical integration error, since they are removed by using the finer (99, 590) integration grid. The Pt═Pt distance of 2.645 Å (BP86) or 2.637 Å

dx.doi.org/10.1021/ic5005243 | Inorg. Chem. 2014, 53, 5300−5310

(MPW1PW91) in **25S-1** is significantly shorter than any of the Pt−Pt single bond distances in the $Pt_2(PF_3)_n$ (n = 7, 6) structures and thus can be interpreted as a formal double bond. This gives the Pt atom in the $Pt(PF_3)_3$ unit the favored 18-electron configuration but the Pt atom in the $Pt(PF_3)$ unit only a 16-electron configuration, considering the Pt═Pt double bond to be polarized, with a positive charge on the $Pt(PF_3)_3$ unit and a negative charge on the $PtPF_3$ unit.

The unbridged $Pt_2(PF_3)_5$ structure **25S-2** consists of $Pt(PF_3)_3$ and $Pt(PF_3)_2$ units linked by a formal Pt═Pt double bond of length 2.707 Å (BP86 or MPW1PW91) (Figure 5 and Table 3). This gives the $Pt(PF_3)_3$ platinum atom in **25S-2** the favored 18-electron configuration but the $Pt(PF_3)_2$ platinum atom only a 16-electron configuration.

The C_{3v} unbridged $Pt_2(PF_3)_5$ structure **25S-3** consists of a $Pt(PF_3)_4$ unit coordinating to a $Pt(PF_3)$ unit with a Pt═Pt double bond of length 2.614 Å (BP86) or 2.622 Å (MPW1PW91) (Figure 5 and Table 3). Structure **25S-3** can be considered as a substitution product of $Pt(PF_3)_2$ in which one of the PF_3 ligands has been replaced with a $Pt(PF_3)_4$ ligand. Thus, the $Pt(PF_3)_4$ platinum atom has the favored 18-electron configuration, and the $Pt(PF_3)$ platinum atom has a 16-electron configuration if the $Pt(PF_3)_4$ platinum atom contributes all four electrons to the Pt═Pt double bond. Structure **25S-3** has four small imaginary vibrational frequencies of 30*i*, 30i, 25*i*, and 10*i* cm^{-1} (BP86), or 26*i*, 21*i*, 21*i*, and 5*i* cm^{-1} (MPW1PW91).

3.3.4. $Pt_2(PF_3)_4$. Two $Pt_2(PF_3)_4$ structures were found (Figure 6 and Table 4). The lower-energy structure **24S-1** consists of a $Pt(PF_3)_2$ unit and a $Pt(PF_3)$ unit linked by a direct Pt═Pt bond and a bridging PF_3 group. This bridging PF_3 group is an unprecedented type bonded to the central Pt_2 unit not only by Pt−P bonds (~2.4 Å) but also by two weak F→Pt dative bonds (~3.0 Å) to the $Pt(PF_3)$ unit. Thus, this bridging PF_3 group is an effective six-electron donor $\eta^{3,1}$-μ-PF_3 ligand, with five of these electrons going to the $Pt(PF_3)$ unit and the sixth electron to the $Pt(PF_3)_2$ unit. The Pt═Pt distance 2.649 Å (BP86) or 2.640 Å (MPW1PW91) can be interpreted as a formal double bond. Placing a formal positive charge on the $Pt(PF_3)$ platinum atom and a formal negative charge on the $Pt(PF_3)_2$ platinum atom gives each platinum atom the favored 18-electron configuration.

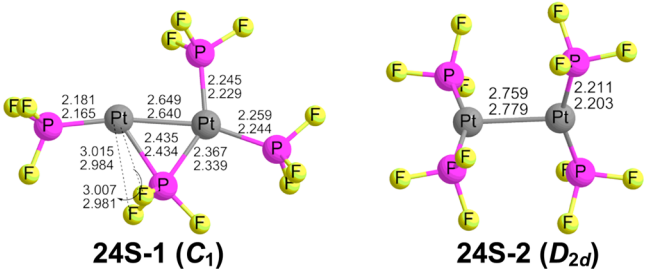

Figure 6. The two optimized $Pt_2(PF_3)_4$ structures.

Table 4. Selected Data for the Two Optimized $Pt_2(PF_3)_4$ Structures

		24S-1 (C_1)	**24S-2** (D_{2d})[a]
BP86	E[b]	−2803.474 45	−2803.466 17
	ΔE[c]	0.0	5.2
	gap[d]	2.47	2.02
	Pt−Pt[e]	2.649	2.759
	N_{imag}[f]	none	5(18*i*,10*i*,10*i*,9*i*,6*i*)
MPW1PW91	E	−2802.923 08	−2802.911 94
	ΔE	0.0	7.0
	gap	4.37	3.59
	Pt−Pt	2.640	2.779
	N_{imag}	none	3(30*i*,3*i*,3*i*)

[a]A single imaginary frequency of 19*i* cm^{-1} (BP86) or 30*i* cm^{-1} (MPW1PW91) was obtained by using the finer integration grid (99, 590). [b]Total energies (E in Hartree). [c]Relative energies (ΔE in kcal/mol). [d]HOMO−LUMO gaps (in eV). [e]Pt−Pt distances (in Å). [f]Numbers of imaginary vibrational frequencies.

The other low-energy $Pt_2(PF_3)_4$ structure **24S-2**, lying 5.2 kcal/mol (BP86) or 7.0 kcal/mol (MPW1PW91) above **24S-1**, is an unbridged structure with D_{2d} symmetry and five (BP86) or three (MPW1PW91) small imaginary vibrational frequencies (Figure 6 and Table 4). However, the number of imaginary vibrational frequencies is reduced to one, that is, 19*i* cm^{-1} (BP86) or 30*i* cm^{-1} (MPW1PW91), when the finer integration grid (99, 590) is used. Following the normal mode corresponding to this single imaginary vibrational frequency lowers the energy by 1.4 kcal/mol, with relatively little change in the geometry but reduction in symmetry to give a C_2 structure.

3.4. Structures of the Trinuclear Derivative $Pt_3(PF_3)_6$. Four $Pt_3(PF_3)_6$ structures were optimized (Figure 7 and Table 5). The lowest-energy structure **36S-1** is a C_1 structure consisting of two $Pt(PF_3)_2$ units and one $Pt(PF_3)$ unit, with the sixth PF_3 group bridging all three Pt atoms of the Pt_3 triangle as an η^2-μ_3-PF_3 ligand using the phosphorus atom and one of the fluorine atoms. The three Pt−Pt distances in **36S-1** are 2.671, 2.702, and 2.829 Å (BP86) or 2.666, 2.680, and 2.815 Å (MPW1PW91), suggesting two formal Pt═Pt double bonds and a formal Pt−Pt single bond. The unprecedented unsymmetrical bridging η^2-μ_3-PF_3 group forms two short Pt−P bonds of 2.402 and 2.411 Å (BP86) or 2.364 and 2.435 Å (MPW1W91) and one long Pt−P bond of 2.863 Å (BP86) or 2.855 Å (MPW1W91) to the three platinum atoms of the Pt_3 triangle in **36S-1**. However, the η^2-μ_3-PF_3 group also forms

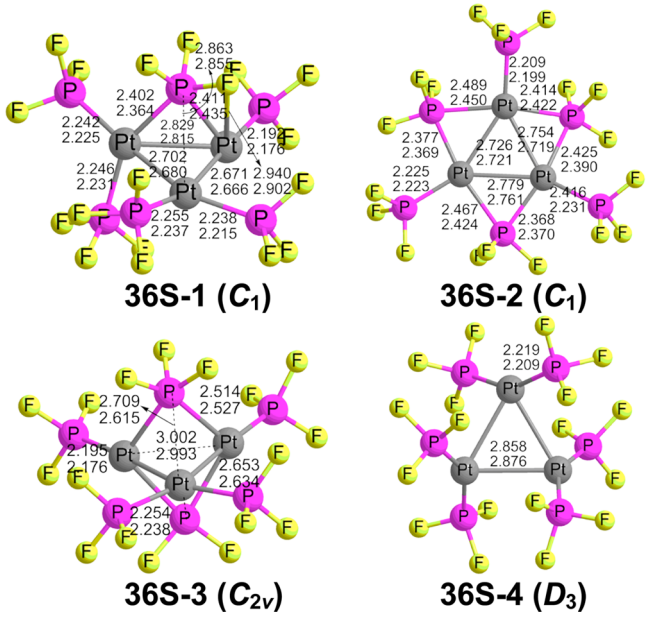

Figure 7. The four optimized $Pt_3(PF_3)_6$ structures.

dx.doi.org/10.1021/ic5005243 | Inorg. Chem. 2014, 53, 5300−5310

Table 5. Selected Data for the $Pt_3(PF_3)_6$ Structures

		36S-1 (C_1)	36S-2 (C_1)	36S-3 (C_{2v})[a]	36S-4 (D_3)[a]
BP86	E[b]	−4205.243 64	−4205.237 59	−4205.232 36	−4205.220 73
	ΔE[c]	0.0	3.8	7.1	14.4
	gap[d]	2.51	2.52	2.71	1.73
	Pt−Pt[e]	2.829, 2.702, 2.671	2.754, 2.726, 2.779	2.653, 2.653, 3.002	2.858
	N_{img}[f]	none	none	3(16*i*,15*i*,4*i*)	2(13*i*,13*i*)
MPW1PW91	E	−4204.416 59	−4204.410 46	−4204.399 15	−4204.388 74
	ΔE	0.0	3.8	10.9	17.5
	gap	4.31	4.40	4.62	3.41
	Pt−Pt	2.815, 2.680, 2.666	2.721,2.719, 2.761	2.634, 2.634, 2.993	2.876
	N_{img}	none	none	2(17*i*,17*i*)	2(16*i*,16*i*)

[a]The imaginary frequencies of these structures are removed by using the finer (99, 590) integration grid. [b]Total energies (E in Hartree). [c]Relative energies (ΔE in kcal/mol). [d]HOMO−LUMO gap (in eV). [e]Pt−Pt distances (in Å). [f]Numbers of imaginary frequencies.

a F→Pt dative bond of length 2.940 Å (BP86) or 2.902 Å (MPW1PW91) and thus is a four-electron donor to the Pt_3 triangle. The combination of two formal Pt═Pt double bonds in the Pt_3 triangle and the four-electron donor η^2-μ_3-PF_3 group gives each platinum atom in **36S-1** the favored 18-electron configuration.

The second lowest-energy $Pt_3(PF_3)_6$ structure **36S-2** lies 3.8 kcal/mol (BP86 or MPW1PW91) above **36S-1** (Figure 7 and Table 5). Each platinum atom bears a terminal PF_3 group, and each Pt═Pt bond in the Pt_3 triangle is bridged by a PF_3 group. Interpreting the ∼2.75 Å Pt═Pt distances in **36S-2** as formal double bonds gives each platinum atom the favored 18-electron configuration.

The $Pt_3(PF_3)_6$ structure **36S-3**, lying 7.1 kcal/mol (BP86) or 10.9 kcal/mol (MPW1PW91) in energy above **36S-1**, has C_{2v} symmetry with two μ_3-PF_3 groups unsymmetrically bridging all three platinum atoms (Figure 7 and Table 5). Thus, the central Pt_3P_2 unit in **36S-3** forms a trigonal bipyramid, with the platinum atoms in equatorial positions and the phosphorus atoms in axial positions (Figure 7 and Table 5). The Pt−Pt distances in **36S-3** are predicted to be 2.653, 2.653, and 3.002 Å (BP86) or 2.634, 2.634, and 2.993 Å (MPW1PW91), suggesting two formal Pt═Pt double bonds and one Pt−Pt single bond. Structure **36S-3** has very small imaginary vibrational frequencies of 16*i*, 15*i*, and 4*i* cm^{-1} (BP86) or 17*i* and 17*i* cm^{-1} (MPW1PW91) that become real when the finer (99, 590) integration grid is used.

The $Pt_3(PF_3)_6$ structure **36S-4** is a significantly higher-energy D_3 unbridged structure, lying 14.4 kcal/mol (BP86) or 17.5 kcal/mol (MPW1PW91) in energy above **36S-1** (Figure 7 and Table 5). Structure **36S-4** has three equivalent Pt−Pt bonds of lengths 2.858 Å (BP86) or 2.876 Å (MPW1PW91), suggesting short single bonds. Each Pt atom bears two PF_3 ligands and thus has a 16-electron configuration. The pair of degenerate imaginary vibrational frequencies in **36S-4** (16*i* cm^{-1} by MPW1PW91 or 13*i* cm^{-1} by BP86) is removed by using the finer (99, 590) integration grid.

3.5. Thermochemistry. Table 6 lists energies for PF_3 dissociation from mononuclear and binuclear $PtPF_3$ complexes based on the lowest-energy structures. All of the PF_3 dissociation energies are seen to be significant, with the lowest dissociation energy being the ∼13 kcal/mol dissociation energy of $Pt_2(PF_3)_7$. For both the mononuclear $Pt(PF_3)_n$ and the binuclear $Pt_2(PF_3)_n$ derivatives the PF_3 dissociation energies increase with decreasing numbers of PF_3 groups. These significant PF_3 dissociation energies suggest that all of the species reported in this paper are viable with respect to PF_3 dissociation.

Table 6. Trifluorophosphine Dissociation Energies (in kcal/mol) for Mononuclear and Binuclear Pt-PF_3 Complexes

	ΔE	
	BP86	MPW1PW91
$Pt_2(PF_3)_7$ (**27S-1**) → $Pt_2(PF_3)_6$ (**26S-1**) + PF_3	13.4	18.0
$Pt_2(PF_3)_6$ (**26S-1**) → $Pt_2(PF_3)_5$ (**25S-1**) + PF_3	16.3	16.1
$Pt_2(PF_3)_5$ (**25S-1**) → $Pt_2(PF_3)_4$ (**24S-1**) + PF_3	21.6	24.2
$Pt(PF_3)_4$ (**14S-1**) → $Pt(PF_3)_3$ (**13S-1**) + PF_3	22.4	25.0
$Pt(PF_3)_3$ (**13S-1**) → $Pt(PF_3)_2$ (**12S-1**) + PF_3	26.5	27.3

A major motivation of this research was to examine the energetics of aggregation of $Pt(PF_3)_n$ units to give the experimentally observed $Pt_4(PF_3)_8$. In this connection Table 7 lists the energies for various aggregation processes starting with mononuclear derivatives and leading ultimately to $Pt_4(PF_3)_8$. All of these aggregation processes are seen to be strongly exothermic except for the reaction of $Pt(PF_3)_4$ with $Pt(PF_3)_3$ to give $Pt_2(PF_3)_7$, which is essentially thermoneutral (±2 kcal/mol). Two conclusions can be drawn from this thermochemical information:

(1) The tetramerization of $Pt(PF_3)_2$ to give the experimentally known $Pt_4(PF_3)_8$ is a strongly exothermic process by ∼100 kcal/mol. However, the energy of ∼190 kcal/mol required to convert 4 equiv of $Pt(PF_3)_4$ to $Pt(PF_3)_3$ and then $Pt(PF_3)_3$ to $Pt(PF_3)_2$ makes the overall conversion of 4 $Pt(PF_3)_4$ to $Pt_4(PF_3)_8$ + 8 PF_3 endothermic by ∼90 kcal/mol. Therefore, $Pt(PF_3)_4$ is predicted to be viable with respect to PF_3 loss followed by tetramerization to $Pt_4(PF_3)_8$. This is consistent with the known stability of $Pt(PF_3)_4$, which has even been offered commercially.

(2) The dimeric $Pt_2(PF_3)_7$ is not a viable compound, consistent with its essentially thermoneutral fragmentation to $Pt(PF_3)_4$ + $Pt(PF_3)_3$. This also is consistent with the experimentally observed stability of $Pt(PF_3)_4$.

3.6. Natural Bond Orbital Analysis. Tables 8 and 9 report the Weinhold natural charges on the platinum atoms, Pt−Pt distances, Wiberg bond indices (WBIs), and predicted Pt−Pt stretching frequencies for Pt−Pt bonds in the binuclear $Pt_2(PF_3)_n$ (n = 7, 6, 5, and 4) and trinuclear $Pt_3(PF_3)_6$ structures, respectively, using natural bond orbital (NBO) analyses.[25] In connection with the interpretation of the WBIs, metal−metal bonds involving transition metals have been shown generally to have WBIs of only a fraction of the assigned formal bond orders. However, the relative values of WBIs of

dx.doi.org/10.1021/ic5005243 | Inorg. Chem. 2014, 53, 5300−5310

Table 7. Aggregation Energies (in kcal/mol) for Constructing Polynuclear Platinum Trifluorophosphine Complexes

	ΔE	
	BP86	MPW1PW91
$Pt(PF_3)_4$ (**14S-1**) + $Pt(PF_3)_3$ (**13S-1**) → $Pt_2(PF_3)_7$ (**27S-1**)	1.6	−0.6
$Pt(PF_3)_4$ (**14S-1**) + $Pt(PF_3)_2$ (**12S-1**) → $Pt_2(PF_3)_6$ (**26S-1**)	−11.5	−9.9
$2Pt(PF_3)_3$ (**13S-1**) → $Pt_2(PF_3)_6$ (**26S-1**)	−7.5	−7.6
$Pt(PF_3)_3$ (**13S-1**) + $Pt(PF_3)_2$ (**12S-1**) → $Pt_2(PF_3)_5$ (**25S-1**)	−17.6	−18.9
$2Pt(PF_3)_2$ (**12S-1**) → $Pt_2(PF_3)_4$ (**24S-1**)	−22.5	−22.0
$3Pt(PF_3)_2$ (**12S-1**) → $Pt_3(PF_3)_6$ (**36S-1**)	−53.8	−53.1
$4Pt(PF_3)_2$ (**12S-1**) → $Pt_4(PF_3)_8$ (**48S-1**)	−104.2	−103.3
$2Pt_2(PF_3)_4$ (**24S-1**) → $Pt_4(PF_3)_8$ (**48S-1**)	−59.2	−59.3

Table 8. Wiberg Bond Indices (WBI)

structures	natural charge on Pt/Pt	WBI[a]	Pt−Pt distance (Å)	ν(Pt−Pt) (cm^{-1})	formal Pt−Pt bond order	bridging groups
27S-1	−0.25/−0.21	0.08	3.025	84	1	none
27S-2	−0.22/−0.20	0.10	2.931	90	1	PF_3
26S-1	−0.31/−0.31	0.05	3.090	62	0	none
26S-2	−0.29/−0.21	0.09	2.862	91	1	none
26S-3	−0.32/−0.20	0.07	2.920	90	1	none
25S-1	−0.22/−0.34	0.17	2.645	119	2	PF_3
25S-2	−0.27/−0.33	0.14	2.707	106	2	none
25S-3	−0.41/−0.20	0.15	2.614	122	2	none
24S-1	−0.34/−0.28	0.21	2.649	124	2	PF_3
24S-2	−0.47/−0.47	0.12	2.759	103	0	none

[a]Indices (BP86 method) for the Pt−Pt bonds and natural charges on the platinum atoms for the singlet $Pt_2(PF_3)_n$ (n = 7, 6, 5, and 4) structures.

Table 9. Wiberg Bond Indices (WBI)

structures	natural charge on Pt/Pt/Pt	WBI[a]	Pt−Pt distance (Å)	formal Pt−Pt bond order
36S-1	−0.25/−0.30/−0.31	0.12/0.19/0.16	2.829/2.702/2.671	1/2/2
36S-2	−0.26/−0.24/−0.25	0.15/0.14/0.15	2.754/2.779/2.726	2/2/2
36S-3	−0.24/−0.24/−0.26	0.08/0.16/0.16	3.002/2.653/2653	1/2/2
36S-4	−0.42/−0.42/−0.42	0.09/0.09/0.09	2.858/2.858/2.858	1/1/1

[a]Indices (BP86 method) for the Pt−Pt bonds and natural charges on the platinum atoms for the singlet $Pt_3(PF_3)_6$ structures.

transition metal−metal bonds are consistent with the formal bond orders as inferred from metal−metal distances, electron counting, etc. For example, in binuclear binary iron carbonyl systems the WBI for the triply bridged presumed Fe−Fe bond in $Fe_2(CO)_9$ is only 0.11.[45] Even for a hypothetical unbridged triangular structure of $Fe_3(CO)_{12}$, the WBIs for the three equivalent unbridged Fe−Fe bonds are only 0.18.

This same trend continues for the WBIs of the Pt−Pt bonds in the $Pt_2(PF_3)_n$ (n = 7, 6, 5, and 4) and trinuclear $Pt_3(PF_3)_6$ structures, except the WBIs for a Pt−Pt bond of a given order are even lower than those for an Fe−Fe bond of the same order. Thus, the Pt-PF_3 complexes with a formal Pt−Pt single bond generally have WBIs ranging from 0.07 to 0.10. The WBIs for the Pt═Pt double bonds in the $Pt_2(PF_3)_5$ and $Pt_3(PF_3)_6$ structures are consistently higher, ranging from 0.12 to 0.21. The WBI for the unusual Pt−Pt interaction in the lowest-energy $Pt_2(PF_3)_6$ structure **26S-1** is abnormally low at 0.05, indicating a very small contribution of direct Pt−Pt bonding to hold together the two $Pt(PF_3)_3$ halves of this molecule. This is consistent with the relatively low dissociation energy of ∼7.5 kcal/mol for $Pt_2(PF_3)_6$ to give 2 $Pt(PF_3)_3$.

The natural charges on the Pt atoms in the Pt-PF_3 complexes depend only very weakly on the number of PF_3 groups bonded to the platinum atom in question, as compared with metal−carbonyl derivatives, where increasing the numbers of CO groups consistent leads to a more negative charge on the metal atom (Tables 8 and 9). Thus, the negative charges on the platinum atoms in the entire series of trifluorophosphine complexes studied in this research with various numbers of PF_3 groups bonded to each platinum atom fall in the narrow range from −0.20 to −0.47. This suggests that the back bonding of filled platinum d orbitals to antibonding orbitals of the PF_3 ligands is more effective at removing the negative charge arising from the forward σ bonding than is the case with metal−carbonyl complexes.

The ν(Pt−Pt) frequencies of 158, 134, and 110 cm^{-1} have been observed by Raman spectroscopy for the Pt−Pt single bond in the binuclear platinum(III) phosphite complexes $[Pt_2(pop)_4X_2]^{4-}$ (pop = $P_2O_5H_2$; X = Cl, Br, I).[46] In our work, where the platinum local environment is consistent with a +1 rather than a +3 effective oxidation state, the ν(Pt−Pt) frequencies are lower for a given bond order. Thus, in $Pt_2(PF_3)_n$ with formal Pt−Pt single bonds, the ν(Pt−Pt) frequencies range from 84 to 90 cm^{-1}. However, for the $Pt_2(PF_3)_5$ derivatives with formal Pt═Pt double bonds, the ν(Pt═Pt) frequencies are distinctly higher, ranging from 103 to 124 cm^{-1}.

3.5. Frontier Molecular Orbital Analysis of the Unbridged $Pt_2(PF_3)_6$ and $Pt_2(PF_3)_4$ Structures. Figure 8 shows the frontier MOs for the unbridged $Pt_2(PF_3)_6$ structure **26S-1**, namely, the MOs from LUMO down to HOMO−9. The bonding MOs from HOMO−7 down to HOMO−9 in

dx.doi.org/10.1021/ic5005243 | Inorg. Chem. 2014, 53, 5300−5310

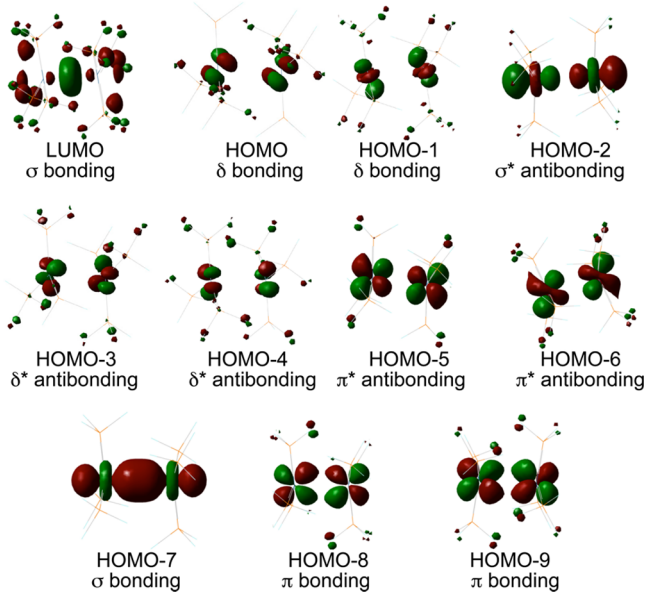

Figure 8. The frontier bonding molecular orbitals from LUMO down to HOMO−9 in the unbridged $Pt_2(PF_3)_6$ structure **26S-1** (Figure 4).

26S-1 (Figure 4) are seen to correspond to the σ component and two π components of a Pt≡Pt triple bond. However, the HOMO, HOMO−5, and HOMO−6 MOs correspond to σ^* antibonding and two π^* antibonding components of the platinum−platinum interaction, thereby canceling out all three components of such a Pt≡Pt triple bond. This observation suggests that there is no net σ or π bonding between the two platinum atoms in **26S-1**. Furthermore, HOMO−1 and HOMO−2 bonding MOs in **26S-1**, corresponding to two δ bonding components at 45° to each other, are canceled out by the HOMO−3 and HOMO−4 δ^* antibonding MOs (Figures 8 and 9). Thus, the formal bond order of the Pt−Pt interaction in

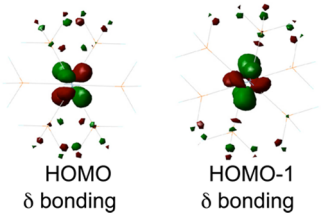

Figure 9. A view of HOMO and HOMO−1 looking down the S_6 axis of the $Pt_2(PF_3)_6$ structure **26S-1**. This view shows the ∼45° angle between HOMO and HOMO−1.

26S-1 is effectively zero. However, configuration interaction with the pσ and pσ^* orbitals can stabilize the dσ^* and dσ levels, resulting in net favorable interactions.[47] This is consistent with the unusual position of the δ^* antibonding orbitals lying in energy below the δ bonding orbitals. A similar type of Pt−Pt interaction has been suggested in platinum(II) diimine complexes with a linear chain structure.[48] The predicted Pt−Pt distance of ∼3.1 Å in **26S-1** is only slightly shorter than the experimental 3.2 to 3.5 Å Pt−Pt distances in the linear chain platinum(II) diimine complexes. The weakness of the Pt−Pt interaction in **26S-1** is indicated by the low predicted energy of ∼7.5 kcal/mol for the dissociation of the unbridged $Pt_2(PF_3)_6$ structure **26S-1** into two $Pt(PF_3)_3$ fragments (Table 7) as well as the low WBI of 0.05.

The LUMO for the neutral $Pt_2(PF_3)_6$ structure corresponds to σ bonding. The corresponding dianion $Pt_2(PF_3)_6^{2-}$ (**26S-1**)$^{2-}$ has the same S_6 symmetry as the neutral **26S-1** (Figure 10) and lies significantly below the neutral **26S-1** by ∼59 kcal/

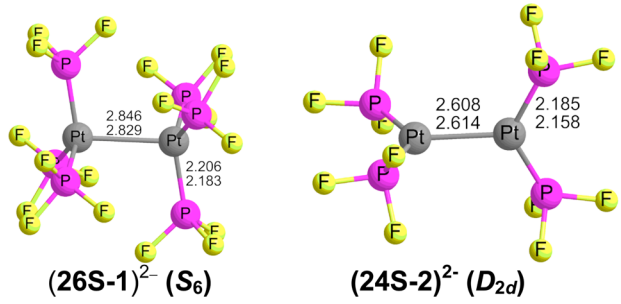

Figure 10. The optimized $Pt_2(PF_3)_6^{2-}$ and $Pt_2(PF_3)_4^{2-}$ dianion structures.

mol, suggesting a substantial electron affinity for **26S-1**. Adding two electrons to the LUMO of **26S-1** upon reduction to the dianion (**26S-1**)$^{2-}$ corresponds to a formal Pt−Pt σ bond, resulting in a significantly shorter Pt−Pt distance of 2.846 Å (BP86) or 2.829 Å (MPW1PW91) relative to the ∼3.1 Å Pt−Pt distance in neutral **26S-1**. Such a formal Pt−Pt single bond gives each Pt atom the favored 18-electron configuration in the dianion $Pt_2(PF_3)_6^{2-}$ (**26S-1**)$^{2-}$.

Figure 11 shows the frontier MOs for the unbridged $Pt_2(PF_3)_4$ structure **24S-2**. The situation appears to be

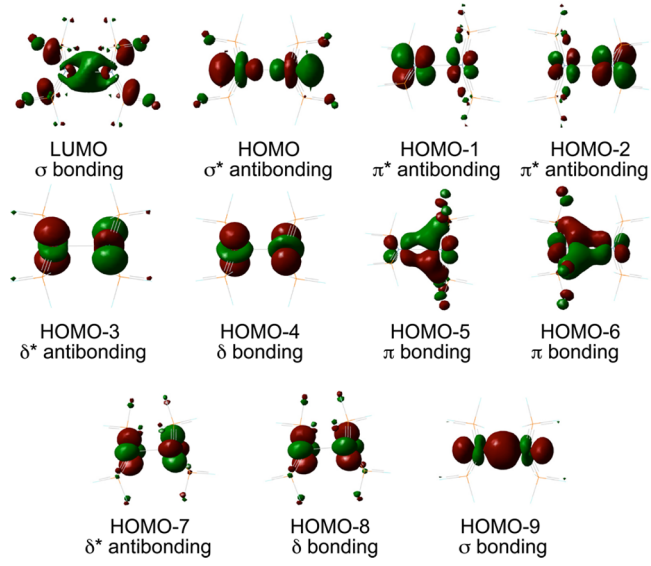

Figure 11. The frontier bonding molecular orbitals from LUMO down to HOMO−9 in the unbridged $Pt_2(PF_3)_4$ structure **24S-2** (Figure 6).

analogous to that for the unbridged $Pt_2(PF_3)_6$ structure **26S-1** discussed above. Thus, the HOMO−9, HOMO−6, and HOMO−5 bonding MOs corresponding to the σ and two π components of a Pt≡Pt triple bond in **24S-2** are canceled out by the HOMO, HOMO−1, and HOMO−2 MOs, which correspond to σ^* antibonding and two π^* antibonding components of the platinum−platinum interaction. This again suggests the absence of net σ or π bonding between the two platinum atoms in the $Pt_2(PF_3)_4$ structure **24S-2**. Similarly, HOMO−4 and HOMO−8, corresponding to the δ bonding

dx.doi.org/10.1021/ic5005243 | Inorg. Chem. 2014, 53, 5300−5310

components of a Pt−Pt bond, are canceled out by the corresponding HOMO−3 and HOMO−7 δ^* antibonding orbitals. However, the Pt−Pt interaction in **24S-2** is relatively strong with a Pt−Pt distance of ∼2.76 Å and a WBI of 0.12, which are comparable to the formal Pt−Pt single bonds in **26S-2** and **26S-3** (Table 8). In addition the dissociation energy of the $Pt_2(PF_3)_4$ structure **24S-2** into 2 $Pt(PF_3)_2$ is significant at ∼22 kcal/mol.

The LUMO in the neutral unbridged $Pt_2(PF_3)_4$ structure **24S-2**, like that in the neutral unbridged $Pt_2(PF_3)_6$ structure **26S-1**, corresponds to σ bonding. The corresponding dianion $Pt_2(PF_3)_4^{2-}$ $(\mathbf{24S\text{-}2})^{2-}$ has the same D_{2d} symmetry as the neutral **24S-2** (Figure 10) and lies 39.8 kcal/mol in energy below **24S-2**, indicating a substantial electron affinity. With the LUMO (σ bonding orbital) of neutral **24S-2** doubly occupied, thereby adding a σ component to the Pt−Pt interaction, the dianion $(\mathbf{24S\text{-}2})^{2-}$ has a shorter Pt−Pt bond of length 2.608 Å (BP86) or 2.614 Å (MPW1PW91) than that in neutral **24S-2**.

4. DISCUSSION

The tetranuclear derivative $Pt_4(PF_3)_8$ is of particular interest since it was synthesized in 1997[17] but never characterized structurally, owing to difficulties in obtaining suitable single crystals for X-ray crystallography. Our theoretical study strongly suggests a distorted tetrahedral structure **48S-1** for $Pt_4(PF_3)_8$ with all terminal PF_3 groups and retaining beautiful S_4 symmetry (Figure 1). Structure **48S-1** was found to be the lowest-energy $Pt_4(PF_3)_8$ structure by more than 20 kcal/mol. Simple electron counting by the Wade−Mingos rules[49−51] has a $Pt(PF_3)_2$ vertex contributing two skeletal electrons like the ^{t}BuB vertex in the experimentally known[52] tetrahedral tetraborane $^t Bu_4B_4$ (^{t}Bu = *tert*-butyl) so that these systems have eight skeletal electrons by the Wade−Mingos rules. This would correspond to a three-center Pt_3 bond in each of the four faces of the Pt_4 tetrahedron. However, the six edges of the Pt_4 tetrahedron in the $Pt_4(PF_3)_8$ structure **48S-1** are not all of the same length so that the structure has S_4 rather than T_d symmetry. Thus, four of the six Pt═Pt edges in **48S-1** have lengths of ∼2.6 Å, suggesting formal double bonds, whereas the other two Pt−Pt edges are ∼0.3 Å longer at ∼2.9 Å, suggesting formal single bonds. Formulating the Pt_4 tetrahedron in **48S-1** with four Pt═Pt double bonds and two Pt−Pt single bonds plays havoc with electron counting using the Wade−Mingos rules[49−51] and suggests a bonding scheme different from that of the apparently valence-isoelectronic tetraborane[52] $^t Bu_4B_4$. We rationalize these observations by interpreting the apparently tetrahedral $Pt_4(PF_3)_8$ as based on a central doubly bonded Pt_4 square, so that each platinum atom has the favored 18-electron configuration from the two PF_3 groups and two Pt═Pt double bonds to adjacent platinum atoms. However, this Pt_4 square is flexible enough to bend along the diagonals through weaker metallophilic Pt−Pt interactions[53] related to those suggested for the $Pt_2(PF_3)_6$ structure **26S-1** (Figures 4 and 12). The resulting central Pt_4 configuration looks like a tetrahedron, but in terms of the metal−metal interactions it can be better interpreted as a distorted square squeezed along each diagonal.

The structures of the lower-nuclearity species $Pt(PF_3)_n$ (n = 4, 3, 2), $Pt_2(PF_3)_n$ (n = 7, 6, 5, 4), and $Pt_3(PF_3)_6$ were investigated to assess their possible roles as possible intermediates in the formation of $Pt_4(PF_3)_8$ by the pyrolysis of $Pt(PF_3)_4$. The preferred structures for the central PtP_n units in the mononuclear $Pt(PF_3)_n$ (n = 4, 3, 2) derivatives (Figure 2) approximate the expected geometries of tetrahedral for n = 4 in **14S-1**, trigonal planar for n = 3 in **13S-1**, and linear for n = 2 in **12S-1**. However, the PtP_2 coordination in the $Pt(PF_3)_2$ structure **12S-1** deviates somewhat from linearity, with a P−Pt−P angle of ∼160°.

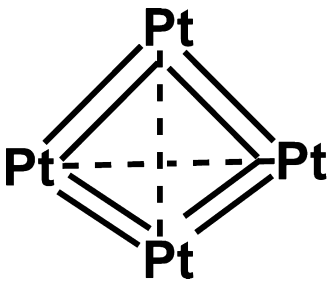

Figure 12. Distortion of a doubly bonded Pt_4 square in $Pt_4(PF_3)_8$ to form a Pt_4 tetrahedron through metallophilic interactions along the diagonals of the square. The metallophilic interactions are represented by dashed lines, and the PF_3 groups are omitted for clarity.

Many of the low-energy structures of the binuclear $Pt_2(PF_3)_n$ derivatives (n = 7, 6, 5, 4) can be dissected into a $Pt(PF_3)_m$ unit (m = mainly 4 but also 3) acting as a "ligand" toward an unsaturated $Pt(PF_3)_n$ (n = 3, 2, 1) unit through a platinum lone pair, sometimes with one of the PF_3 groups in the ligand bending over to bridge to the other platinum atom. In such species the Pt−Pt bonds have considerable dative character, reflecting electron donation from the ligand platinum atom in $Pt(PF_3)_4$ or $Pt(PF_3)_3$. Thus, either low-energy $Pt_2(PF_3)_7$ structure **27S-1** or **27S-2** (Figure 3) can be dissected into a $Pt(PF_3)_4$ ligand bonding to a $Pt(PF_3)_3$ unit, either without a bridging PF_3 group (**27S-1**) or with one of the PF_3 groups in the $Pt(PF_3)_4$ ligand bridging to the other platinum atom (**27S-2**). Alternatively and equivalently, these two $Pt_2(PF_3)_7$ structures can be derived from $Pt(PF_3)_4$ by replacing one of the PF_3 groups with a $Pt(PF_3)_4$ ligand. However, in either of these $Pt_2(PF_3)_7$ structures the binding of the $Pt(PF_3)_4$ ligand to the $Pt(PF_3)_3$ is essentially thermoneutral (Table 7), so that $Pt(PF_3)_4$ is a weak ligand in these $Pt_2(PF_3)_7$ structures. Therefore, $Pt_2(PF_3)_7$ is a very fragile species not likely to be synthesized as a stable molecule.

Two of the three low-energy $Pt_2(PF_3)_6$ structures can similarly be derived from the mononuclear $Pt(PF_3)_3$ by replacing one of the PF_3 groups with a $Pt(PF_3)_4$ ligand. In **26S-2** one of the PF_3 groups of the $Pt(PF_3)_4$ ligand bridges the other platinum atom, whereas in **26S-3** all of the PF_3 groups remain terminal groups (Figure 4). However, the lowest-energy $Pt_2(PF_3)_6$ structure **26S-1** is of a different type, constructed from two $Pt(PF_3)_3$ units linked by a weak Pt−Pt interaction as supported by a very low WBI of 0.05 (Figures 8 and 9). The weakness of the Pt−Pt interaction in **26S-1** is supported by the low predicted energy of only ∼7.5 kcal/mol for the dissociation of $Pt_2(PF_3)_6$ into 2 $Pt(PF_3)_3$.

The three low-energy $Pt_2(PF_3)_5$ structures can similarly be interpreted as a $Pt(PF_3)_4$ or $Pt(PF_3)_3$ ligand bonded to a $PtPF_3$ or $Pt(PF_3)_2$ unit, respectively (Figure 5). Structures **25S-1** and **25S-3** can be derived from $Pt(PF_3)_2$ by replacement of one of the PF_3 groups with a $Pt(PF_3)_4$ ligand with or without a single bridging PF_3 group, respectively. The remaining low-energy $Pt_2(PF_3)_5$ structure **25S-2** can analogously be derived from $Pt(PF_3)_3$ by replacement of one of the PF_3 groups with a $Pt(PF_3)_3$ ligand.

Two low-energy $Pt_2(PF_3)_4$ structures were found (Figure 6). The lowest-energy $Pt_2(PF_3)_4$ structure **24S-1** can be derived

dx.doi.org/10.1021/ic5005243 | Inorg. Chem. 2014, 53, 5300−5310

from $Pt(PF_3)_2$ by replacing one of the PF_3 groups with a $Pt(PF_3)_3$ ligand. In **24S-1** the bridging PF_3 group is unusual since it becomes an effective six-electron donor by forming two dative F → Pt bonds with the platinum atom bearing only one terminal PF_3 group. The other $Pt_2(PF_3)_4$ structure **24S-2** consists of two $Pt(PF_3)_2$ units linked by a Pt═Pt double bond, as suggested by comparison of the WBI of 0.12 for this Pt═Pt interaction with the WBIs of other Pt−Pt interactions interpreted as either formal single or double bonds (Table 8).

Comparison of the preferred structures of the binuclear platinum trifluorophosphine complexes $Pt_2(PF_3)_n$ (n = 6, 5, 4) with their previously studied[54] nickel analogues indicates a lower tendency of the platinum derivatives to form structures with bridging PF_3 groups than the corresponding nickel derivatives. Thus, both low-energy $Ni_2(PF_3)_6$ structures are predicted to have two bridging PF_3 groups with normal Ni−P distances. However, the low-energy $Pt_2(PF_3)_6$ structures have zero (**26S-1**), one (**26S-2**), or two very weakly bridging PF_3 groups (**26S-3**), with short Pt−P distances of ∼2.3 Å and long Pt−P distances of ∼2.8 Å. Similarly all three low-energy $Ni_2(PF_3)_5$ structures have either one or two bridging PF_3 groups, whereas only one of the three low-energy structures, namely **25S-1** (Figure 5), has a single bridging PF_3 group. For $Ni_2(PF_3)_4$ two of the three low-energy structures have two bridging PF_3 groups, whereas for $Pt_2(PF_3)_4$ one of the two low-energy structures has a single bridging PF_3 group. This greater tendency of first-row transition metals to form structures with bridging ligands in polynuclear complexes relative to third-row transition metals is well-known in metal−carbonyl chemistry. Thus, $Fe_2(CO)_9$ has a structure with three bridging CO groups,[55,56] whereas $Os_2(CO)_9$ has a structure with a single bridging CO group.[57,58] Similarly $Co_4(CO)_{12}$ has a structure with three bridging CO groups,[59] whereas $Ir_4(CO)_{12}$ has exclusively terminal CO groups.[60]

The four low-energy $Pt_3(PF_3)_6$ structures all have central Pt_3 triangles. In **36S-2** and **36S-4** these Pt_3 triangles are nearly equilateral. In **36S-2** each edge of the Pt_3 triangle is bridged by a PF_3 group leaving only a single terminal PF_3 group for each platinum atom. However, in **36S-4** all six PF_3 groups are terminal and distributed equally between the three platinum atoms to give a triangle of $Pt(PF_3)_2$ units. The remaining two $Pt_3(PF_3)_6$ structures **36S-1** and **36S-3** have approximately isosceles Pt_3 triangles, with two short Pt═Pt distances interpreted as formal double bonds and one longer Pt−Pt distance interpreted as a formal single bond. Structure **36S-1** has an unusual four-electron donor η^2-μ_3-PF_3 group bridging the Pt_3 triangle forming Pt−P bonds to all three platinum atoms and a F→Pt dative bond to one of the platinum atoms. Structure **36S-3** has two μ_3-PF_3 groups bridging the Pt_3 triangle to form a distorted Pt_3P_2 trigonal bipyramid with the phosphorus atoms in axial positions.

The predicted energetics of the formation of $Pt_4(PF_3)_8$ via aggregation of Pt-PF_3 complexes of lower nuclearity is of interest since $Pt_4(PF_3)_8$ has been found as a pyrolysis product of $Pt(PF_3)_4$ in platinum deposition studies.[17] The thermochemical data in Table 7 suggest that after two PF_3 groups are driven out from $Pt(PF_3)_4$ by pyrolysis or photolysis, the tetramerization of the resulting $Pt(PF_3)_2$ to $Pt_4(PF_3)_8$ is a highly exothermic process, regardless of the involvement of species of intermediate nuclearity such as $Pt_2(PF_3)_4$ or $Pt_3(PF_3)_6$.

5. SUMMARY

The experimentally known but structurally uncharacterized $Pt_4(PF_3)_8$ is predicted to have a central distorted Pt_4 tetrahedron exhibiting S_4 symmetry with four short Pt═Pt distances, two long Pt−Pt distances, and all terminal PF_3 groups. The structures of the lower-nuclearity species $Pt(PF_3)_n$ (n = 4, 3, 2), $Pt_2(PF_3)_n$ (n = 7, 6, 5, 4), and $Pt_3(PF_3)_6$ were investigated to assess their roles as possible intermediates in the formation of $Pt_4(PF_3)_8$ by the pyrolysis of $Pt(PF_3)_4$. The expected tetrahedral, trigonal planar, and linear structures are found for $Pt(PF_3)_4$, $Pt(PF_3)_3$, and $Pt(PF_3)_2$, respectively. However, the dicoordinate $Pt(PF_3)_2$ structure is bent from the ideal 180° linear structure to approximately 160°. Most of the low-energy binuclear $Pt_2(PF_3)_n$ (n = 7, 6, 5) structures can be derived from the $Pt(PF_3)_n$ (n = 4, 3, 2) structures by replacing one of the PF_3 groups with a $Pt(PF_3)_4$ or $Pt(PF_3)_3$ ligand. In some of these binuclear structures one of the PF_3 groups on the $Pt(PF_3)_n$ ligand becomes a bridging group. Low-energy binuclear structures also include symmetrical unbridged $[Pt(PF_3)_n]_2$ dimers (n = 2, 3) of the coordinately unsaturated $Pt(PF_3)_n$ (n = 3, 2).

Four low-energy structures were found for the trinuclear $Pt_3(PF_3)_6$. Two of these structures have central Pt_3 equilateral triangles with either all terminal PF_3 groups or with three of the six PF_3 groups bridging the Pt−Pt triangle edges. The other two $Pt_3(PF_3)_6$ structures have central Pt_3 isosceles triangles, with two short Pt═Pt distances and one longer Pt−Pt distance. One of these structures has a four-electron donor η^2-μ_3-PF_3 bridging the Pt_3 triangle by forming Pt−P bonds with each platinum atom and a dative F→Pt bond to one of the platinum atoms. The other such structure has two μ_3-PF_3 groups bridging both the top and bottom of the central Pt_3 triangle, forming a Pt_3P_2 trigonal bipyramid.

Studies of the thermochemistry of aggregation of Pt-PF_3 complexes suggest that the tetramerization of $Pt(PF_3)_2$ to $Pt_4(PF_3)_8$ is highly exothermic regardless of the mechanistic details.

■ ASSOCIATED CONTENT

Supporting Information

Tables S1 to S7: total energies (E, in Hartree), relative energies (ΔE, in kcal/mol), relative energies corrected by ZPE (ΔE_{ZPE}, in kcal/mol), numbers of imaginary frequencies (N_{img}) for the optimized structures of $Pt_n(PF_3)_m$ (n = 1−4, m = 2−8) by the BP86 and MPW1PW91 methods; Tables S8 to S14: harmonic vibrational frequencies (cm^{-1}) and corresponding infrared intensities (in parentheses) predicted by BP86 for the optimized structures $Pt(PF_3)_n$ (n = 4, 3, and 2), $Pt_2(PF_3)_n$ (n = 7, 6, 5, and 4), $Pt_3(PF_3)_6$, and $Pt_4(PF_3)_8$; Tables S15: the $\nu(PF_3)$ stretching frequencies predicted for the mononuclear $Pt(PF_3)_n$ (n = 4, 3, and 2) by BP86; Tables S16 to S19: the $\nu(PF_3)$ stretching frequencies predicted for the binuclear $Pt_2(PF_3)_n$ (n = 7, 6, 5, and 4) by BP86; Table S20: the $\nu(PF_3)$ stretching frequencies predicted for the trinuclear $Pt_3(PF_3)_6$ by BP86; Table S21: the $\nu(PF_3)$ stretching frequencies predicted for the tetranuclear $Pt_4(PF_3)_8$ by BP86; Tables S22 to S30: Cartesian coordinates for the optimized structures $Pt(PF_3)_n$ (n = 4, 3, and 2), $Pt_2(PF_3)_n$ (n = 7, 6, 5, and 4), $Pt_3(PF_3)_6$, and $Pt_4(PF_3)_8$ by BP86 and MPW1PW91; Complete Gaussian 09 reference (ref 39).This material is available free of charge via the Internet at http://pubs.acs.org.

dx.doi.org/10.1021/ic5005243 | Inorg. Chem. 2014, 53, 5300−5310

AUTHOR INFORMATION

Corresponding Authors

*E-mail: rbking@chem.uga.edu (R.B.K.).
*E-mail: luoqiong@scnu.edu.cn (Q.L.).

Notes

The authors declare no competing financial interest.

ACKNOWLEDGMENTS

We are indebted to the Guangdong Province Universities and Colleges, the National Natural Science Foundation (21273082) of China, and the U.S. National Science Foundation (Grants CHE-1057466 and CHE-1054286) for financial support of this research.

REFERENCES

(1) Green, J. C.; King, D. I.; Eland, J. H. D. *Chem. Commun.* **1970**, 1121.
(2) Hillier, I. H.; Saunders, V. R.; Ware, M. J.; Bassett, P. J.; Lloyd, D. R.; Lynaugh, N. *Chem. Commun.* **1970**, 1316.
(3) Bassett, P. J.; Higginson, B. R.; Lloyd, D. R.; Lynaugh, N.; Roberts, P. J. *J. Chem. Soc., Dalton Trans.* **1974**, 2316.
(4) Müller, J.; Fenderl, K.; Mertschenk, B. *Ber. Bunsen-Ges.* **1971**, *104*, 700.
(5) Head, R. A.; Nixon, J. F.; Sharp, G. J.; Clark, R. J. *J. Chem. Soc., Dalton Trans.* **1975**, 2054.
(6) Nixon, J. F.; Seddon, E. A.; Suffolk, R. J.; Taylor, M. J.; Green, J. C.; Clark, R. J. *J. Chem. Soc., Dalton Trans.* **1986**, 765.
(7) Savariault, J.-M.; Serafini, A.; Pellissier, M.; Cassoux, P. *Theor. Chim. Acta* **1976**, *42*, 155.
(8) Braga, M. *Inorg. Chem.* **1985**, *24*, 2702.
(9) Braga, M. *J. Mol. Struct.* **1992**, *85*, 167.
(10) Frenking, G.; Wichmann, K.; Fröhlich, N.; Grobe, J.; Golla, W.; Le Van, D.; Krebs, B.; Läge, M. *Organometallics* **2002**, *21*, 2921.
(11) Kruck, T. *Angew. Chem., Int. Ed.* **1967**, *6*, 53.
(12) Nixon, J. F. *Adv. Inorg. Chem.* **1985**, *21*, 41.
(13) Rand, M. *J. Electrochem. Soc.* **1973**, *120*, 686.
(14) Morabito, J. M.; Rand, M. J. *Thin Solid Films* **1974**, *22*, 293.
(15) O'Regan, C.; Lee, A.; Holmes, J. D.; Petkov, N.; Trompenaars, P.; Mulders, H. *J. Vac. Sci. Technol., B* **2013**, *31*, 021807/1.
(16) Elbadawi, C.; Toth, M.; Lobo, C. J. *ACS Appl. Mater. Interfaces* **2013**, *5*, 9372.
(17) Hammill, C. L.; Clark, R. J.; Ross, C. W.; Marshall, A. G.; Schmutz, J. *Inorg. Chem.* **1997**, *36*, 5973.
(18) Langmuir, I. *Science* **1921**, *54*, 59.
(19) Bose, D. M. *Z. Phys.* **1926**, 219.
(20) Reiff, F. *Z. Anorg. Allg. Chem.* **1931**, *202*, 375.
(21) Sidgwick, N. V.; Bailey, R. W. *Proc. R. Soc. London* **1934**, *A144*, 521.
(22) Pyykkö, P. *J. Organomet. Chem.* **2006**, *691*, 4336.
(23) Ugo, R.; La Monica, G.; Carlati, F.; Cenini, S.; Conti, F. *Inorg. Chim. Acta* **1970**, *4*, 390.
(24) Ziegler, T.; Autschbach, J. *Chem. Rev.* **2005**, *105*, 2695.
(25) Bühl, M.; Kabrede, H. *J. Chem. Theory Comput.* **2006**, *2*, 1282.
(26) Brynda, M.; Gagliardi, L.; Widmark, P. O.; Power, P. P.; Roos, B. O. *Angew. Chem., Int. Ed.* **2006**, *45*, 3804.
(27) Sieffert, N.; Bühl, M. *J. Am. Chem. Soc.* **2010**, *132*, 8056.
(28) Schyman, P.; Lai, W.; Chen, H.; Wang, Y.; Shaik, S. *J. Am. Chem. Soc.* **2011**, *133*, 7977.
(29) Adams, R. D.; Pearl, W. C.; Wong, Y. O.; Zhang, Q.; Hall, M. B.; Walensky, J. R. *J. Am. Chem. Soc.* **2011**, *133*, 12994.
(30) Lonsdale, R.; Olah, J.; Mulholland, A. J.; Harvey, J. N. *J. Am. Chem. Soc.* **2011**, *133*, 15464.
(31) Becke, A. D. *Phys. Rev. A* **1988**, *38*, 3098.
(32) Perdew, J. P. *Phys. Rev. B* **1986**, *33*, 8822.
(33) Adamo, C.; Barone, V. *J. Chem. Phys.* **1998**, *108*, 664.
(34) Zhao, S.; Wang, W.; Li, Z.; Liu, P.; Fan, K.; Xie, Y.; Schaefer, H. F. *J. Chem. Phys.* **2006**, *124*, 184102.
(35) Andrae, D.; Haussermann, U.; Dolg, M.; Stoll, H.; Preuss, H. *Theor. Chim. Acta* **1990**, *77*, 123.
(36) Dunning, T. H. *J. Chem. Phys.* **1970**, *53*, 2823.
(37) Huzinaga, S. *J. Chem. Phys.* **1965**, *42*, 1293.
(38) Dunning, T. H.; Hay, P. In *Modern Theoretical Chemistry;* Schaefer, H. F., Ed.; Plenum Press: New York, 1977; Vol. 3.
(39) Frisch, M. J.; et al. *Gaussian 09,* Revision A.02; Gaussian, Inc.: Wallingford, CT, 2009; see Supporting Information for details.
(40) Papas, B. N.; Schaefer, H. F. *J. Mol. Struct.* **2006**, *768*, 175.
(41) Jacobsen, H.; Ziegler, T. *J. Am. Chem. Soc.* **1996**, *118*, 4631.
(42) Martin, J. M. L.; Bauschlicher, C. W.; Ricca, A. *Comput. Phys. Commun.* **2001**, *133*, 189.
(43) Paschoal, D.; Marcial, B. L.; Lopes, J. F.; De Almeida, W. B.; Dos Santos, H. F. *J. Comput. Chem.* **2012**, *33*, 2292.
(44) Ritz, C. L.; Bartell, L. S. *J. Mol. Struct.* **1976**, *31*, 73.
(45) Wang, H.; Xie, Y.; King, R. B.; Schaefer, H. F. *J. Am. Chem. Soc.* **2006**, *128*, 11376.
(46) Che, C. M.; Schaefer, W. P.; Gray, H. B.; Dickson, M. K.; Stein, P.; Roundhill, D. M. *J. Am. Chem. Soc.* **1982**, *104*, 4253.
(47) Krogmann, K. *Angew. Chem., Int. Ed.* **1969**, *8*, 35.
(48) Connick, W. B.; Marsh, R. E.; Schaefer, W. P.; Gray, H. B. *Inorg. Chem.* **1997**, *36*, 913.
(49) Wade, K. *Chem. Commun.* **1971**, 792.
(50) Mingos, D. M. P. *Nature (London), Phys. Sci.* **1972**, *99*, 236.
(51) Mingos, D. M. P. *Acc. Chem. Res.* **1984**, *17*, 311.
(52) Mennekes, T.; Paetzold, P.; Boese, R.; Blaeser, D. *Angew. Chem.* **1991**, *103*, 199.
(53) Pyykkö, P. *Chem. Rev.* **1997**, *97*, 597.
(54) Yang, H.-q.; Li, Q.-s.; Xie, Y.; King, R. B.; Schaefer, H. F. *J. Phys. Chem. A* **2010**, *114*, 8896.
(55) Powell, H. M.; Ewens, R. V. G. *J. Chem. Soc.* **1939**, 286.
(56) Cotton, F. A.; Troup, J. M. *J. Chem. Soc., Dalton Trans.* **1974**, 800.
(57) Moss, J. R.; Graham, W. A. G. *Chem. Commun.* **1970**, 835.
(58) Moss J. R.; Graham W. A. G. *J. Chem. Soc., Dalton Trans.* **1977**, 95.
(59) Wei, C. H.; Dahl, L. F. *J. Am. Chem. Soc.* **1966**, *88*, 1821.
(60) Churchill, M. R.; Hutchinson, J. P. *Inorg. Chem.* **1978**, *17*, 3528.